



Experimental determination of stripping foil thickness on the XiPAF synchrotron

Xiao-Yu Liu^{1,2,3} · Hong-Juan Yao^{1,2,3} · Shu-Xin Zheng^{1,2,3} · Ze-Jiang Wang^{1,2,3} · Yang Xiong^{1,2,3} · Pei-Zhi Fang^{1,2,3} · Zhong-Ming Wang⁴

Received: 25 December 2023 / Revised: 7 April 2024 / Accepted: 13 May 2024 / Published online: 29 January 2025

© The Author(s), under exclusive licence to China Science Publishing & Media Ltd. (Science Press), Shanghai Institute of Applied Physics, the Chinese Academy of Sciences, Chinese Nuclear Society 2024

Abstract

Stripping injection overcomes the limitations of Liouville's theorem and is widely used for beam injection and accumulation in high-intensity synchrotrons. The interaction between the stripping foil and beam is crucial in the study of stripping injection, particularly in low-energy stripping injection synchrotrons, such as the XiPAF synchrotron. The foil thickness is the main parameter that affects the properties of the beam after injection. The thin stripping foil is reinforced with collodion during its installation. However, the collodion on the foil surface makes it difficult to determine its equivalent thickness, because the mechanical measurements are not sufficiently reliable or convenient for continuously determining foil thickness. We propose an online stripping foil thickness measurement method based on the ionization energy loss effect, which is suitable for any foil thickness and does not require additional equipment. Experimental studies were conducted using the XiPAF synchrotron. The limitation of this method was examined, and the results were verified by comparing the experimentally obtained beam current accumulation curves with the simulation results. This confirms the accuracy and reliability of the proposed method for measuring the stripping foil thickness.

Keywords Stripping injection · Foil thickness · Synchrotron · Injection efficiency · Experimental study

1 Introduction

Stripping injection overcomes the limitations of Liouville's theorem and is widely used for beam injection and accumulation in high-intensity hadron synchrotrons [1–6] and in some compact synchrotrons [7–11]. The Xi'an 200 MeV Proton Application Facility (XiPAF) is the first facility in China that is dedicated to simulating environments containing space radiation [12–18]. The facility consists of a 7 MeV

linac injector and compact 200 MeV synchrotron. A 7 MeV H^- beam is stripped into a proton beam [19], which is accumulated and accelerated to an extraction energy range of 10–200 MeV. The proton beam is then extracted using a third-order resonance slow-extraction method. The layout of the synchrotron is shown in Fig. 1.

The injection system is crucial in the design of the XiPAF synchrotron. The injection system (Fig. 2) consists of three chicane magnets and one stripping foil, which are all located in the same drift section. Additionally, two injection bump magnets located in the neighboring super-periods are used for injection painting in the horizontal phase space. The magnetic field of the chicane magnets remains constant, whereas that of the injection bump magnets gradually decreases from its maximum value to zero, following the injection bump orbit curve during the injection painting process. Owing to the low energy of the injected beam, the thickness of the stripping foil in the XiPAF synchrotron is designed to be 25 nm, corresponding to a mass thickness of $5 \mu\text{g}/\text{cm}^2$. This minimizes the impact of multiple scattering and ionization energy loss on the beam quality. Because a

✉ Shu-Xin Zheng
zhengsx@tsinghua.edu.cn

¹ Key Laboratory of Particle & Radiation Imaging, Tsinghua University, Beijing 100084, China

² Laboratory for Advanced Radiation Sources and Application, Tsinghua University, Beijing 100084, China

³ Department of Engineering Physics, Tsinghua University, Beijing 100084, China

⁴ National Key Laboratory of Intense Pulsed Radiation Simulation and Effect, Northwest Institute of Nuclear Technology, Xi'an 710024, China

Fig. 1 (Color online) XiPAF synchrotron lattice layout

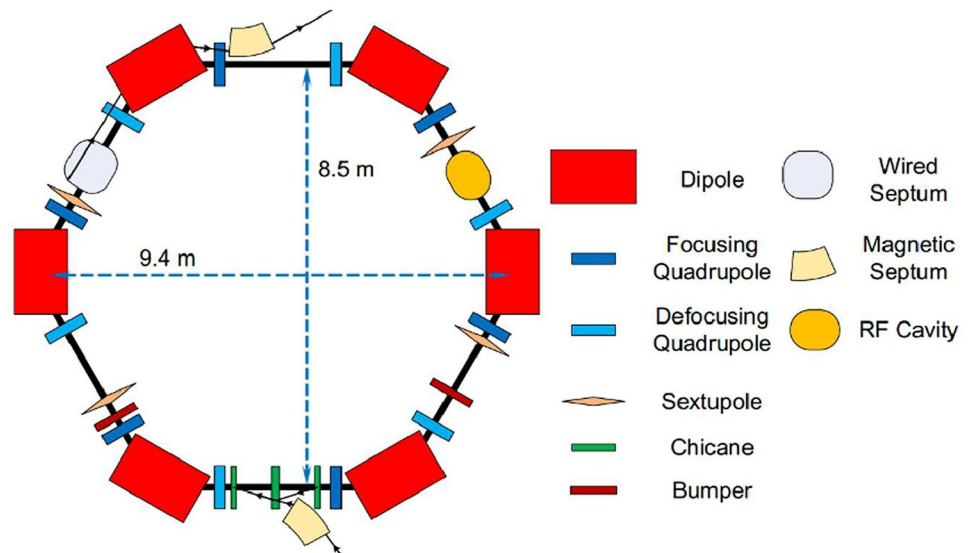
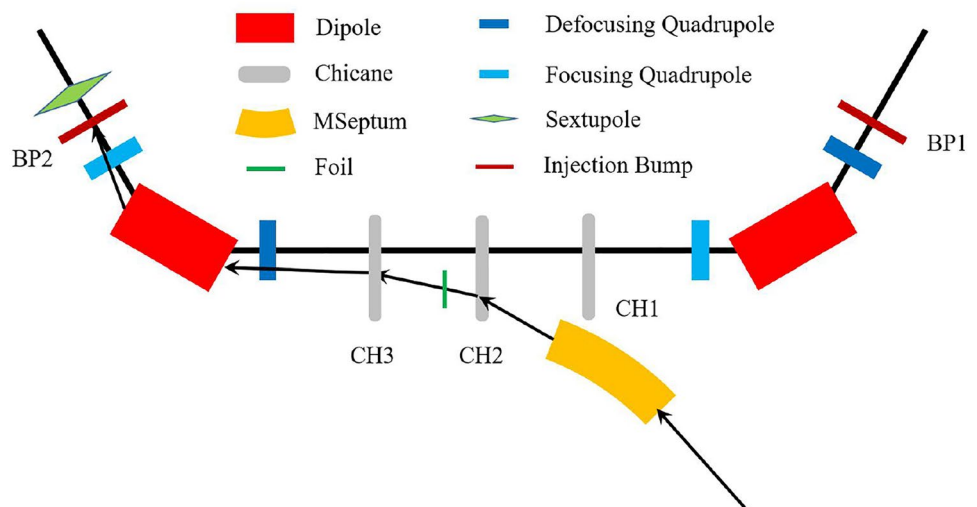


Fig. 2 (Color online) Layout of the XiPAF synchrotron injection system



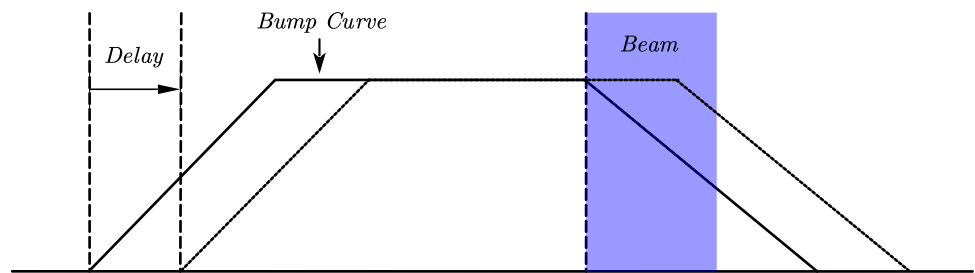
stripping foil with such a small thickness is fragile; it must be strengthened with collodion and mounted onto the stripping foil holder.

The XiPAF synchrotron beam commissioning began in January 2020 [12, 13, 17], and after several rounds of iterative optimization, the optimal injection efficiency was 58%. Simulations performed using the PyORBIT code showed that an injection efficiency of 77% could be achieved under the same beam current conditions, which was significantly higher than the experimental measurements [20, 21].

The experimental results demonstrated that the injection efficiency was highly sensitive to the average foil hit of each circulating proton. The average foil hit was controlled by adjusting the delay of the injection bumper curve during the experiment, as shown in Fig. 3. A larger bump-curve delay results in the injection of a higher proportion of the beam

into the flat-top section of the bump curve, which leads to a higher average foil hit of the circulating proton beam. The simulation results showed an initial rapid increase in the injection efficiency with an increasing average foil hit number, followed by a gradual decrease. However, the experimental measurements differed from the simulation predictions: the injection efficiency initially increased rapidly with the average foil hit number, which was consistent with the simulation results, and then rapidly decreased [21]. The simulation was verified by comparing the PyORBIT [22, 23] and FLUKA [24] codes for low-energy proton beams; the major drawback of the original foil tracking algorithm in the PyORBIT code was the lack of a long tail in the energy distribution. However, this discrepancy was not primarily responsible for the disparity between the simulation and experimental results. The inconsistency between the actual

Fig. 3 (Color online) The foil hit number can be controlled by adjusting the delay of the bump curve



and nominal thicknesses of the stripping foil was main factor contributing to the low injection efficiency. The actual equivalent thickness of the stripping foil was much larger than the nominal value owing to the presence of the collodion on the foil surface, which was used to reinforce the foil. The equivalent thickness of the collodion was unknown, making it challenging to determine the equivalent thickness of the foil.

Previous studies primarily used offline and online measurement methods to determine the foil thickness. Offline methods include (1) using a precision micrometer for mechanical measurement [25], (2) measuring the transmittance of normally incident, monochromatic light [26], (3) using the convergent beam electron diffraction technique [27], (4) using high energy resolution alpha spectroscopy to detect the energy loss of alpha particles as they pass through the foil [28], and (5) directly measuring the quality of the stripping foil. However, all these methods require the removal of the foil from the accelerator, which does not allow continuous measurement of the thickness change. The online method is based on stripping-efficiency measurement, as mentioned in the J-PARC study [29]; however, it requires a high-precision current detector and new beamline for stripping-efficiency measurement. Therefore, it is only suitable for cases where the stripping foil is relatively thin. It is inapplicable in cases where the actual thickness of the XiPAF is significantly greater than the nominal thickness, and the XiPAF cannot accommodate a new beamline to measure the stripping efficiency.

In this study, we propose a method for measuring the actual equivalent thickness of a stripping foil based on the difference in beam energy before and after the foil. This method has the advantage of continuously measuring changes in foil thickness and is suitable for any thickness without requiring any additional equipment. Experimental measurements using the XiPAF synchrotron confirmed the reliability of this method. The remainder of this paper is organized as follows: Sect. 2 describes the proposed method for measuring the equivalent thickness of a stripped foil by measuring the energy loss through the foil. Section 3 presents the experimental preparation, including the experimental scheme and energy measurement methods. Section 4 presents the experimental results from the XiPAF synchrotron

and their analyses. In Sect. 5, we analyze the limitation and reliability of the proposed method by comparing the simulated and experimental results. Section 6 summarizes the conclusions of the study.

2 Online method for foil thickness measurement

The effect of the stripping foil on the beam can be divided into two parts: transverse scattering and longitudinal ionization energy loss. The transverse scattering effect primarily includes multiple scattering and inelastic scattering, which increase the beam transverse emittance. The longitudinal ionization energy loss effect causes particles to lose energy through interactions with electrons outside the nucleus of the material, which reduces the average energy of the beam in the synchrotron and increases the rms momentum spread. This ionization energy loss effect can be used to determine the thickness of the stripping foil.

The online foil thickness measurement method is based on the ionization-energy-loss effect. Its theoretical basis is the Bethe equation [7, 30], which is given by Eq. (12), where the mass stopping power $\langle -dE/dx \rangle$ is related to the atomic number of the particle z , atomic number of the material Z , mass number of the material A , and particle energy.

$$\left\langle -\frac{dE}{dx} \right\rangle = Kz^2 \frac{Z}{A} \frac{1}{\beta^2} \left[\frac{1}{2} \ln \frac{2m_e c^2 \beta^2 \gamma^2 W_{\max}}{I^2} - \beta^2 - \frac{\delta(\beta\gamma)}{2} \right], \tag{1}$$

$$W_{\max} = \frac{2m_e c^2 \beta^2 \gamma^2}{1 + 2\gamma m_e/M + (m_e/M)^2}. \tag{2}$$

Here, W_{\max} denotes the maximum energy transfer in a single collision; m_e and M are the electron and particle masses, respectively; and I is the mean excitation energy. According to the Thomas–Fermi model, the mean excitation energy can be approximated as $I \approx 10Z$ [eV] [31]. $\delta(\beta\gamma)$ is the density effect correction for the ionization energy loss. For low-energy particles, the density effect can be disregarded.

Because the mass-stop power is related only to the material properties and beam energy, and the energy loss is

considerably smaller than the beam energy itself, the average beam energy loss $\langle \Delta E \rangle$ is proportional to the thickness of the medium d . Theoretically, the actual thickness of the stripping foil can be obtained by measuring the energy loss after beam passing through the stripping foil. However, the particle energy loss of a single foil traversal is small and can be significantly affected by errors in energy measurement. Because the beam circulates in the synchrotron and traverses the foil several times, obtaining the curve of the beam energy loss against the foil hit number N is a more reliable method. The average energy loss when the beam passes through the foil N times is

$$\langle \Delta E \rangle = \left\langle \frac{dE}{dx} \right\rangle \times d \times N. \quad (3)$$

According to Eq. (3), the average energy loss $\langle \Delta E \rangle$ and average foil hit number N exhibit a linear relationship. This process is illustrated in Fig. 4, where a steeper slope of the line is obtained with larger foil thickness. This curve can be experimentally measured, and the equivalent foil thickness d can be obtained from the slopes of the measured curves.

This method was verified through simulations. The energy-loss curve simulated by the PyORBIT code was compared with the theoretical formula shown in Fig. 5; the blue and red curves are based on the Bethe equation and PyORBIT simulated results, respectively. The simulation and theory are consistent, and the deviation originates from the distribution of the number of beams passing through the foil. Linear fitting of the simulated results yielded a foil thickness of $51.0 \mu\text{g}/\text{cm}^2$. The relative error of this method was 2%.

In addition, Eq. (1) indicates that the mass-stopping power is approximately proportional to $1/\beta^2$ at low energies, where $\beta\gamma < 1$. Therefore, a beam traversing a medium of a finite thickness loses more energy as the incident particle energy decreases. For thick foils, the average foil hits of 10

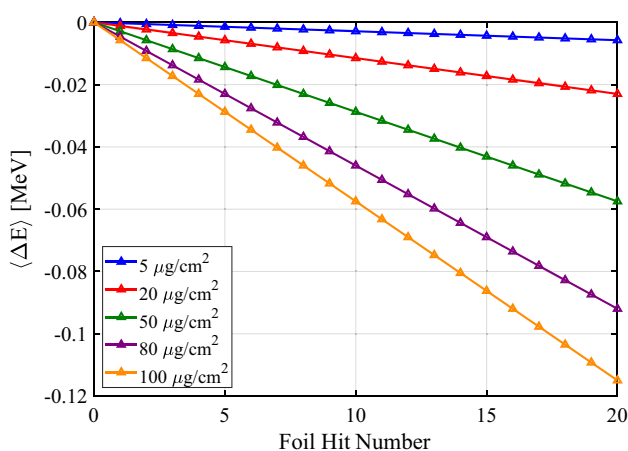


Fig. 4 (Color online) Energy loss changes with the foil hit number

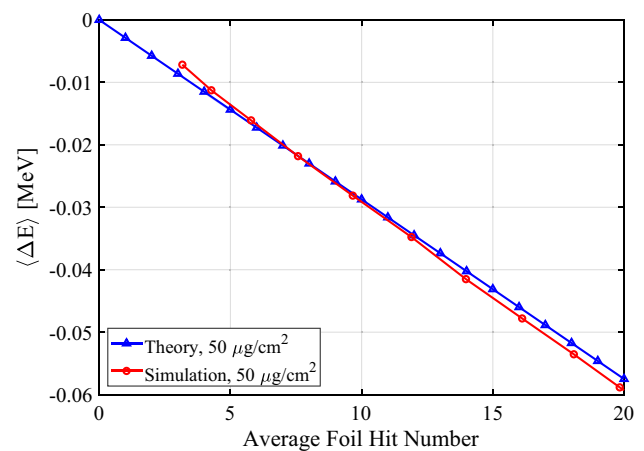


Fig. 5 (Color online) Energy loss changes with the average foil hit number. The blue and red curves are based on the Bethe equation and PyORBIT simulation results, respectively

to 20 can significantly change the beam energy. Higher beam energies or lower foil thicknesses require a higher average foil hit number, and the online measurement method remains reliable.

3 Experimental scheme

3.1 Limitations of using this method on the XiPAF synchrotron

Measurement of the foil thickness on the XiPAF synchrotron using the online method has certain limitations that hinder direct measurement of the foil hit number.

First, this method for measuring the equivalent foil thickness is primarily based on the energy loss curve for different foil hit numbers. Assuming a sufficiently fast decay of the injection bump orbit after a single-turn injection, it can be inferred that the beam no longer passes through the stripping foil, except during the stripping of the negative hydrogen ion beam to a proton beam. Consequently, the average foil hit number increases linearly with the delay of the injection bump curve, as shown in Fig. 3. However, the limited decay rate of the bump magnets makes it impossible to precisely control the foil hit number. The foil hit number and delay of the injection bump curve exhibit a nonlinear relationship.

Second, because the average injected beam current of the XiPAF synchrotron is approximately 0.6 mA, the beam intensity in the ring is insufficient for obtaining signals with a usable signal-to-noise ratio, and the error in the beam energy measurement is unacceptable. To increase the beam intensity in the ring, particles must be accumulated for several turns, resulting in different foil hit numbers for beams injected at different turns. Furthermore, the limited

bump decay rate and transverse betatron motion alter relative position between the particle and stripping foil during the circulation of the beam in the ring. Thus, even particles injected into the ring at the same turn have different foil hit numbers, making it difficult to obtain the curves shown in Fig. 4. Because of the nonzero dispersion function at the injection point, the dispersion orbits of the beam after passing through the stripping foil differ according to the thicknesses. Thus, the subsequent motion and foil hit number of the particle exhibit varying behaviors. Therefore, the relationship between the foil hit number and delay of the injection bump curve depend on the foil thickness.

3.2 Alternative scheme for foil hit number measurement

An alternative scheme was proposed to overcome these problems in the XiPAF synchrotron.

Because the foil hit numbers of the circulating particles were different, the average foil hit number was used. For experimental operation on the XiPAF synchrotron, the average foil hit number was controlled by adjusting the delays of the injection bump curve. Figure 6 illustrates the relationship between the average foil hit number and delay of the injection bump curve, when the injection turn and foil thickness are 6 and 50 $\mu\text{g}/\text{cm}^2$, respectively. The injection bump curve is shown in Fig. 7. The average foil hit number increases with the delay of the injection bump curve; however, the relationship is not linear. This relationship was affected by various factors including the shape of

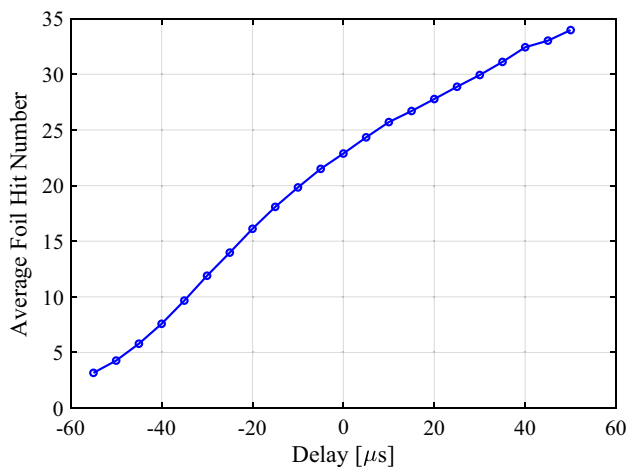


Fig. 6 (Color online) Relation between the average foil hit number and delay of the injection bump curve, when the injection turn and foil thickness are 6 and 50 $\mu\text{g}/\text{cm}^2$, respectively. A delay of 0 μs corresponds to the scenario where the beam injection begins as the bump orbit starts to decrease from the flat-top value to zero. The average foil hit number increases with the injection bump delay, and the slope of the curve decreases

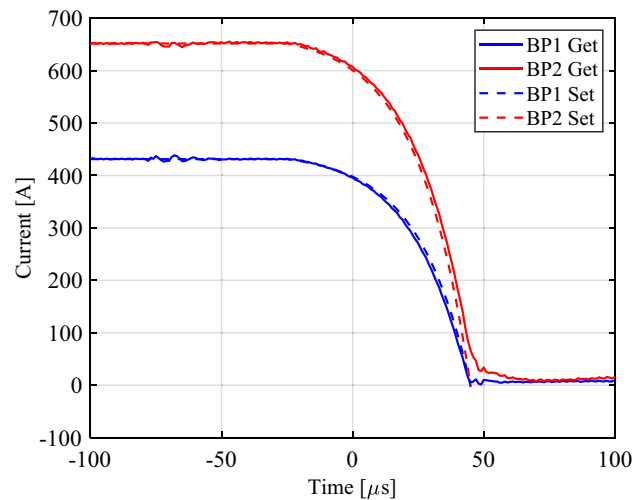


Fig. 7 (Color online) XiPAF synchrotron injection bump current curve. The red and blue lines represent the BP1 and BP2 magnets, respectively. The solid and dashed lines represent the measured and set curves, respectively

the injection bump curve, phase space coordinates of the injected beam, twiss parameters of the injected beam, and thickness of the stripping foil. In the experiment, ensuring a linear relationship between the average foil hit number and the delay of the injection bump curve through the selection of injection parameters was difficult because of the unknown foil thickness. The relationship between the average foil hit number and delay of the injection bump curve could only be obtained through simulations. Therefore, in the experiment, the foil thickness was determined approximately using the delay as an independent variable. Using the simulated relationship between the two at a particular foil thickness, the average foil hit number was calculated from the delay. Linear regression was then applied to the processed data to determine the final foil thickness. The influence of the relationship between the average foil hit number and bump delay is discussed in Sect. 5.

The final scheme for the XiPAF synchrotron experiment is as follows. The injected beam pulse width was set to 5.3 μs , which corresponded to six turns of injections. The beam energies at the medium-energy transport line (MEBT) before injection and in the ring after injection were measured for different delays in the injection bump curve. The equivalent foil thickness was determined by comparing the measured and simulated curves.

3.3 Methods for beam energy measurement

The accurate measurement of the equivalent thickness of the stripping foil depends on the accurate measurement of the beam energy before and after injection.

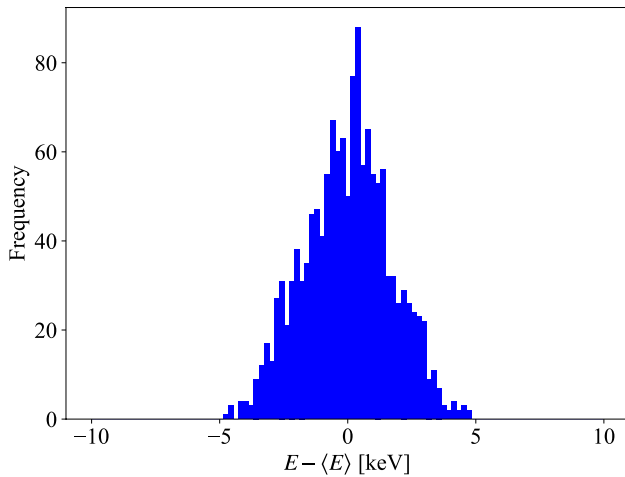


Fig. 8 (Color online) Histogram of the incident beam energy

The beam energy before injection was measured using the time-of-flight (TOF) method [32, 33] with beam position monitors (BPMs) on the MEBT, owing to its pulsed microstructure. In the XiPAF experiment, the beam energy measurement precision exceeded 0.1%; the beam energy at the MEBT exit was stable; and the experimentally measured average incident beam energy was 7.022 MeV. The histogram of the measured beam energy jitter, which was less than 0.005 MeV, is shown in Fig. 8.

The beam energy after injection was measured using the Schottky signal [34, 35]. The Schottky signal, which can be induced at BPM electrodes, provides a nondestructive diagnostic method for synchrotrons. For a particle with charge q and revolution period T_j circulating in a synchrotron, the induced current at a given location in the ring consists of an infinite train of delta functions separated in time by T_j .

$$I_j(t) = q\omega_j \sum_{\ell=-\infty}^{+\infty} \delta(\omega_j t + \theta_j - 2\pi\ell), \tag{4}$$

which can be expressed as a Fourier series:

$$I_j(t) = q \frac{\omega_j}{2\pi} \sum_{m=-\infty}^{+\infty} e^{-im(\omega_j t + \theta_j)}, \tag{5}$$

where $\omega_j = 2\pi f_j = 2\pi/T_j$ and θ_j is the initial phase of the particle. Considering that the initial phases and longitudinal motions of all particles are independent, the induced beam current at a given location is the sum of all N particles.

$$\begin{aligned} I(t) &= \frac{q}{2\pi} \sum_{j=1}^N \sum_{m=-\infty}^{+\infty} \omega_j e^{-im(\omega_j t + \theta_j)} \\ &= q \sum_{j=1}^N f_j + 2q \sum_{j=1}^N \sum_{m=1}^{+\infty} f_j \cos(m\omega_j t + m\theta_j). \end{aligned} \tag{6}$$

This is the longitudinal frequency spectrum [34]; it consists of lines at all harmonics of f_0 , which is the reference frequency corresponding to the beam center energy E_0 of the circulating beam in the synchrotron. Owing to the small frequency deviation or energy deviation of the particles, that is, $\Delta f_j/f_0 \ll 1$ and $\Delta E_j/E_0 \ll 1$, the shape of the Schottky longitudinal spectrum at each harmonic reflects the beam energy distribution. This allows the beam center energy and energy distribution to be determined.

In the experiment, the injection beam pulse width was set to 5.3 μs . The measured beam current curve in the ring from FCT is shown in Fig. 9. Six steps that represent six turns of injection accumulation are observed. The decrease in the beam current after six turns indicates beam loss in the XiPAF synchrotron.

An RSA5100B series real-time signal analyzer was used for Schottky signal measurement. The analyzer was connected to a BPM electrode via an amplifier to acquire the induced beam signal, which provides spectra and spectrograms of the measured signal. These can be saved for beam energy analysis.

The Schottky signal was measured at the harmonic number $m = 2$. Figure 10 shows the Schottky longitudinal spectrum for an injection bump curve delay of $-35 \mu\text{s}$. The blue line represents the measured Schottky spectrum, which is non-Gaussian, asymmetric, and with a tail on the left side owing to the different foil hit numbers for different particles. Because we focused only on the center energy of the

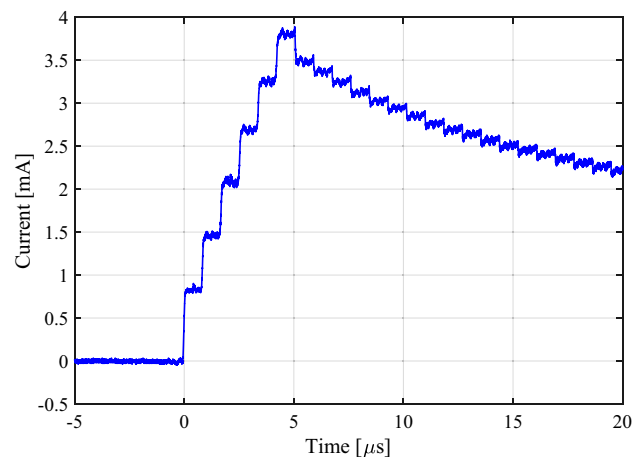


Fig. 9 (Color online) Injection beam current curve with a beam pulse width of 5.3 μs

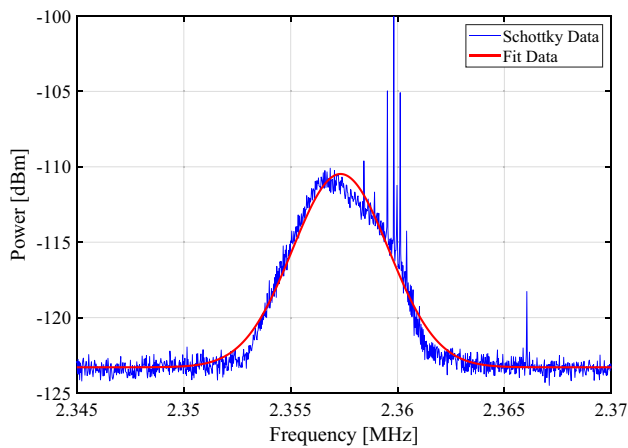


Fig. 10 (Color online) Schottky signal for an injection bump curve delay of $-35 \mu\text{s}$

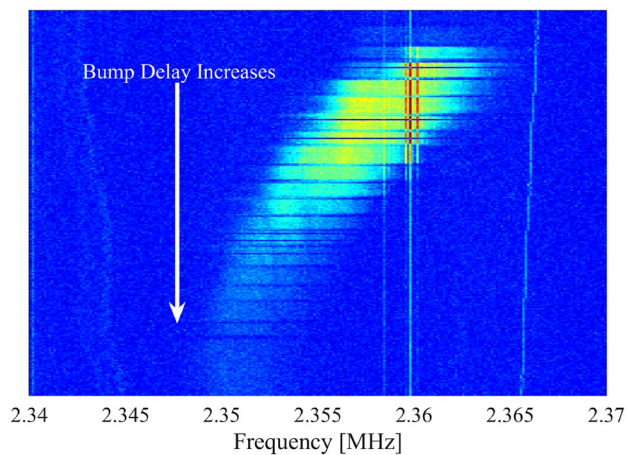


Fig. 11 (Color online) Schottky signal spectrogram for various injection bump curve delays. The horizontal and vertical coordinates represent the frequency, and one sample, respectively, while the colors represent the signal amplitude. Different samples correspond to different delays, and the delay increases from top to bottom. The center frequency of the Schottky signal shifts to the left with increasing delay

beam in the ring, a Gaussian distribution was used to fit the Schottky longitudinal spectrum, as indicated by the red line in Fig. 10. Based on the measured center frequency, the corresponding center energy of the beam current was calculated as 6.989 MeV.

4 Experimental results

The Schottky longitudinal spectra were obtained for all injection bump curve delays. The measured Schottky longitudinal spectrograms for all bump delays are shown in Fig. 11. The horizontal coordinate represents the frequency;

each vertical coordinate corresponds to one Schottky signal sample; and the colors represent the signal amplitude. Different samples correspond to different injection bump curve delays, and the delay gradually increases from top to bottom. The vertical lines in Fig. 11 represent the noise frequencies.

The peak frequency of the Schottky spectrum shifts to the left as the injection bump curve delay increases, indicating an increase in the ionization energy loss. The amplitude of the Schottky signal is proportional to the beam intensity in the ring. As the delay increases, the beam intensity in the ring initially increases and then decreases.

As previously discussed, the equivalent thickness of the stripping foil in the experiment can be determined by comparing the beam energy loss curves measured in the experiment with the simulation results for various foil thicknesses. The incident beam energy was measured as 7.022 MeV using the BPMs at the MEBT, and the center energy of the beam in the ring was determined via Gaussian fitting of the Schottky signal. Subsequently, the curves of energy loss versus injection bump delay were derived from the data, as shown in Fig. 12. The colored and black lines represent the simulation and experimental results, respectively. Measurements were performed for various foils labeled #4, #5, #14, and #28.

Foils #4 and #5 were pure diamond-like carbon foils with a nominal thickness of 500 nm, corresponding to a mass thickness of $100 \mu\text{g}/\text{cm}^2$. Foil #4 was used for 1.5 years, while foil #5 was a new foil. In Fig. 12a, the energy-loss curve of foil #4 is close to the red curve, and its thickness is approximately $50 \mu\text{g}/\text{cm}^2$. After transferring the injection-bump curve delay to the average foil hit number (Fig. 12b), a foil thickness of $52.0 \mu\text{g}/\text{cm}^2$ was calculated by linear fitting. In addition, the measured thickness of foil #5 was $131.4 \mu\text{g}/\text{cm}^2$. Foil #4 exhibited significant foil degradation after being hit by the beam for 1.5 years.

Foils #14 and #28 were the new foils with collodion on their surfaces. The nominal thickness of foil #14 was $5 \mu\text{g}/\text{cm}^2$, whereas the measured mass thickness was $77.5 \mu\text{g}/\text{cm}^2$. The nominal thickness of foil #28 was $7 \mu\text{g}/\text{cm}^2$, whereas the measured mass thickness was $49.2 \mu\text{g}/\text{cm}^2$. No direct relationship was observed between the equivalent and nominal thicknesses. The collodion on the foil surface was primarily responsible for the ionization effect of the stripping foil on the beam.

The beam energy in the synchrotron was measured from the Schottky signal for all harmonic numbers. The consistency of the measured results at different harmonic numbers was verified. Figure 13 shows the differences in the measured curves at different harmonic numbers for foil #4. The measured curves are almost identical and closely match the simulated curve of $50 \mu\text{g}/\text{cm}^2$. A slight difference exists between the edges of these two curves, particularly when the injection bump curve delay is less than $25 \mu\text{s}$. This is

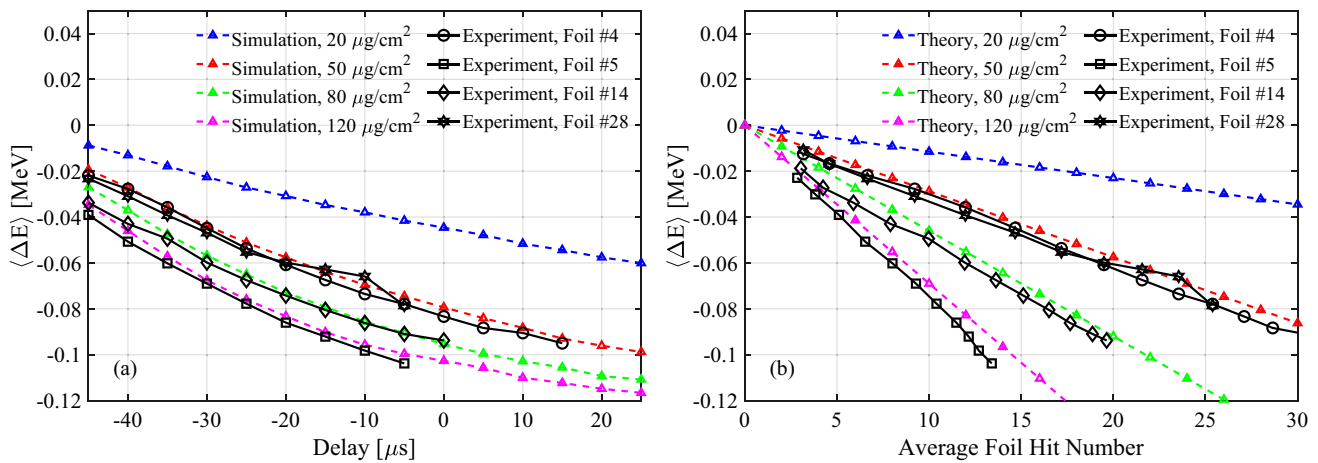


Fig. 12 (Color online) Curves of the energy loss versus injection bump curve delay (a) and average foil hit number (b) for various foils. The colored lines represent the simulation results in (a) or calculated results using Eq. (3) in (b). The black lines represent the experimental results

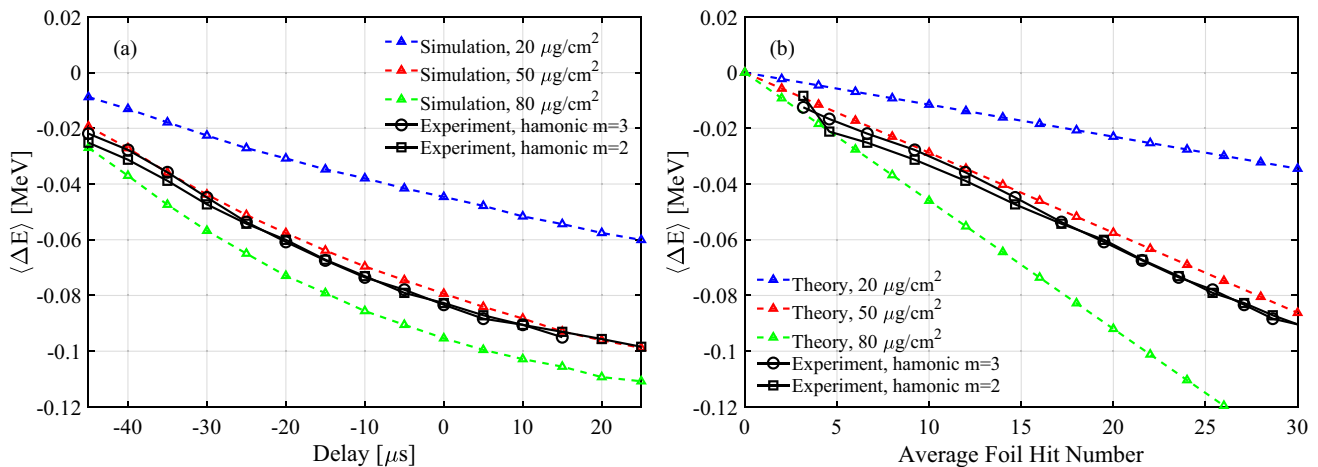


Fig. 13 (Color online) Curve of the energy loss versus injection bump curve delay (a) and average foil hit number (b) for foil #4. The colored and black lines represent the simulation and experimental results, respectively

attributed to the low signal-to-noise ratio for low beam intensities during these delays. The foil thickness measured at harmonic number $m = 3$ was 52.0 μ g/cm², and the thickness measured at harmonic number $m = 2$ was 49.2 μ g/cm². The measurement error was less than 6%.

5 Error analysis and comparison with simulations

In this section, we present the error analysis of the proposed method. For the normal injection mode of the XiPAF synchrotron, the experimental and simulated beam current accumulation curves were compared to verify the validity of the stripping foil thickness measured above. The experimental and simulation results were consistent.

5.1 Error analysis

The proposed method of measuring the equivalent foil thickness is based on the energy loss curve for different foil hit numbers. The foil thickness was determined from the slope of the linear fit between the energy loss and average foil hit numbers, as shown in Fig. 5.

However, for the XiPAF synchrotron, the average foil hit number cannot be directly measured. Instead, the delay of the injection bump curve was used to control the average foil hit number. As previously stated, the average foil hit number was calculated based on the delay in the injection-bump curve, and their relationship was obtained through simulation. The average hit number was calculated for the particles that could be stored in the synchrotron. Owing to the limited momentum acceptance, an increase in the bump curve

delay resulted in the loss of particles that had frequently traversed the foil, and these particles were excluded from the calculation. For a fixed bump curve delay, an increase in foil thickness lowered the average foil hit number, because of the increased energy loss of the particles each time they traversed the foil and limited momentum acceptance. Therefore, the relationship curves between the delay and average foil hit number differed for different thicknesses. To establish this relationship, the measured curves were compared with the simulated curves shown in Fig. 12a. The simulated curve closest to the measured curve was selected to obtain the approximate thickness. Based on this thickness, we established the relationship between the delay and average foil hit number, and then performed a linear fitting to obtain the final foil thickness.

During this process, errors in the foil hit number and energy loss resulted in horizontal and vertical shifts, respectively, as shown in Fig. 12b. The curve shift in Fig. 12b does not affect the foil thickness measurements. However, the shift in the curve shown in Fig. 12a may introduce errors in the approximate thickness measurements. Therefore, the relationship between the delay in the injection bump curve and average foil hit number may be inaccurate, which could affect the final foil thickness measurement results. The discrepancy between the set and actual bump delays was checked, and no errors were found. However, the error in the energy loss arises from the incident beam energy measurement and betatron motion-induced Schottky frequency shift. Thus, the curve in Fig. 12a shifts vertically, which leads to errors in the foil thickness.

$$D = \frac{1}{N} \sum_{j=1}^N (\Delta E_{j,thick1} - \Delta E_{j,thick2}), \quad t_i \leq t_j \leq t_f \quad (7)$$

The curve distance is used to describe the proximity of the two curves in Fig. 12a, as defined in Eq. (7), where t_j is the delay of the injection bump curve; and $\Delta E_{j,thick1}$ and $\Delta E_{j,thick2}$ are the energy losses for different thicknesses at each t_j . For the XiPAF experiment, the thickness was relatively large, and t_f was chosen as 20 μ s owing to momentum acceptance. The distance between the two curves decreases with increasing foil thickness, as shown in Fig. 14. The measurement error in the energy loss resulted in a larger error in the foil thickness measurement. Figure 15 shows the effect of the energy loss error on the foil thickness measurement error for different foil thicknesses. For foil thicknesses larger than 40 μ g/cm², the measurement error increases with the foil thickness. For foil thicknesses less than 40 μ g/cm², the ionization energy loss effect is weak, and the measurement error can be reduced by increasing the injection bump curve delay, which can result in a measurement error of less than 5%/keV.

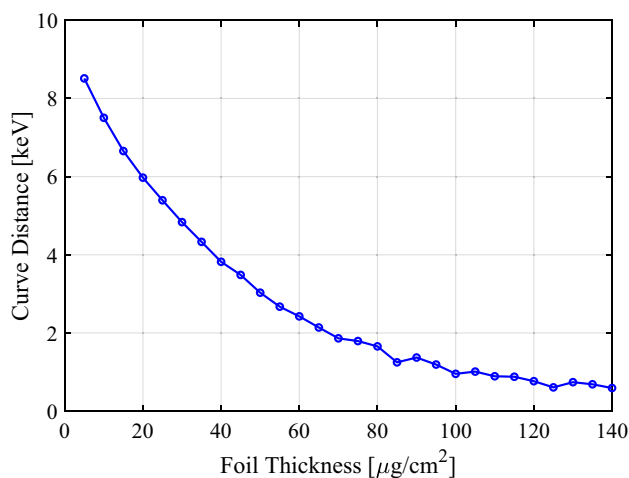


Fig. 14 (Color online) The distance between the two curves in Fig. 12a decreases with increasing foil thickness

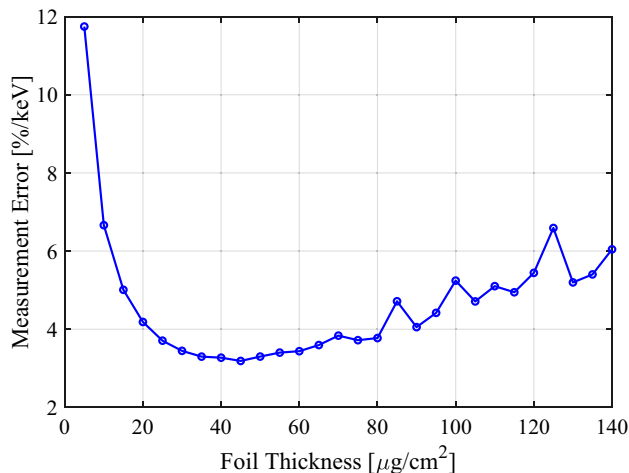


Fig. 15 (Color online) Influence of energy loss error on foil thickness measurement error for different foil thicknesses

In the XiPAF experiment, the beam energy before injection was measured using the TOF method; and the measurement precision and energy jitter were less than 0.1% and 5 keV, respectively. In addition, the dispersion mismatch and betatron motion at the injection point resulted in an energy shift of 0.7 keV. We considered the error in the energy loss to be 5.7 keV, and the thickness measurement error was 21% ~ 32% for foil thicknesses of 50 μ g/cm² ~ 120 μ g/cm², which agreed with the measurement results. The foil thickness measurement error reduced if the foil thickness was small or the momentum acceptance of the synchrotron was sufficiently large.

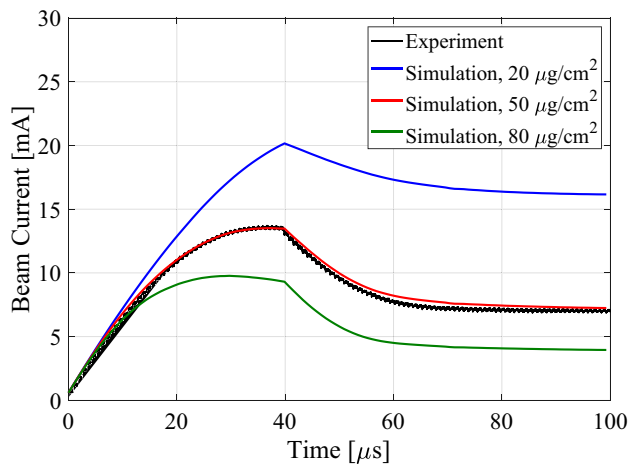


Fig. 16 (Color online) Comparison of beam current accumulation curves. The black line represents the experimental measurement, and the colored lines represent simulation results for various foil thicknesses

5.2 Comparison with simulation results

The stripping foil thickness is a crucial factor that affects the injection efficiency. To ensure the accuracy of the foil thickness measurement results, the simulated beam current accumulation curves were compared with experimental data.

The pulse width of the injection beam for the normal mode of the XiPAF synchrotron was 40 μs and foil #4 was used. The initial beam distribution used in the simulations was generated based on the measured results. In the experiment, the beam current at the MEBT exit varied from a maximum value of 0.6 mA to a final value of 0.3 mA. The simulation considered varying incident beam currents. The space-charge effect was negligible for this beam, which had a large emittance, low intensity, and its influence on the injection efficiency was less than 1%. For foil thicknesses greater than 10 $\mu\text{g}/\text{cm}^2$, the stripping efficiency of the 7 MeV H^- beam was greater than 99.7%; therefore, the stripping efficiency was considered as 100% in the simulations.

Figure 16 shows a comparison of the beam current accumulation curves when the delay of the injection bump curve is set to 0 μs . The black line represents the experimental beam-current curve, whereas the colored lines represent the simulated curves for different foil thicknesses. The measured black curve closely matches the red curve, which represents the simulation results for a foil thickness of 50 $\mu\text{g}/\text{cm}^2$. The experimental and simulated beam accumulation curves are consistent, and the measurement results for the stripping foil thickness are reliable. If the foil thickness is greater than 50 $\mu\text{g}/\text{cm}^2$, the final

accumulated beam current is lower than the measured current, and vice versa.

6 Conclusion

Stripping injection can overcome the limitations of Liouville's theorem, and is a widely used beam injection and accumulation method for high-intensity synchrotrons. The interaction between the stripping foil and beam is crucial in the study of stripping injection, particularly in low-energy synchrotrons, such as the XiPAF. The carbon foil used in the XiPAF synchrotron, which has a nominal thickness of 5 $\mu\text{g}/\text{cm}^2$, is reinforced with collodion to improve its mechanical properties. This results in a significant difference between the actual and nominal thicknesses. This study proposes a method for measuring the equivalent thickness of the stripping foil, based on its ionization energy loss effect. Experimental studies on the XiPAF synchrotron demonstrated the reliability of this method.

The thickness of the stripping foil in the XiPAF synchrotron was measured to be approximately 50 $\mu\text{g}/\text{cm}^2$. The beam current accumulation curves obtained during the injection process were compared with the simulation results. The comparison confirmed the accuracy of the stripping foil thickness measurement results and the reliability of the method.

The large foil thickness was confirmed to be the primary factor contributing to low injection efficiency. Further investigation and optimization are required to improve injection efficiency.

Author contributions All authors contributed to the study conception and design. Material preparation was performed by Hong-Juan Yao, Shu-Xin Zheng and Zhong-Ming Wang. Data collection was performed by Xiao-Yu Liu, Ze-Jiang Wang, Yang Xiong and Pei-Zhi Fang. Data analysis was performed by Xiao-Yu Liu. The first draft of the manuscript was written by Xiao-Yu Liu. The draft was reviewed by Hong-Juan Yao and Shu-Xin Zheng. All authors read and approved the final manuscript.

Data availability The data that support the findings of this study are openly available in Science Data Bank at <https://cstr.cn/31253.11.sciencedb.j00186.00364> and <https://doi.org/10.57760/sciencedb.j00186.00364>.

Declarations

Conflict of interest The authors declare that they have no Conflict of interest.

References

1. J.Y. Tang, Rapid cycling synchrotrons and accumulator rings for high-intensity hadron beams. *Rev. Accel. Sci. Technol.* **6**, 143–169 (2013). <https://doi.org/10.1142/S1793626813300077>

2. G.F. Qu, W.P. Chai, J.W. Xia et al., Two-plane painting injection scheme for BRING of HIAF. *Nucl. Sci. Tech.* **28**, 114 (2017). <https://doi.org/10.1007/s41365-017-0260-5>
3. M.Y. Huang, S.Y. Xu, J. Chen et al., Study on the H⁻ stripping injection for the rapid cycling synchrotron of the China spallation neutron source. *Radiat. Detect. Technol. Methods* **6**, 201–208 (2022). <https://doi.org/10.1007/s41605-022-00326-4>
4. M.Y. Huang, S.Y. Xu, Y.W. An et al., Study on the anti-correlated painting injection scheme for the rapid cycling synchrotron of the China spallation neutron source. *Nucl. Instrum. Methods A* **1007**, 165408 (2021). <https://doi.org/10.1016/j.nima.2021.165408>
5. M.J. Shirakata, H. Fujimori, Y. Irie et al., Particle tracking study of the injection process with field interferences in a rapid cycling synchrotron. *Phys. Rev. ST Accel. Beams* **11**, 064201 (2008). <https://doi.org/10.1103/PhysRevSTAB.11.064201>
6. V.C. Kempson, C.W. Planner, V.T. Pugh et al., Injection dynamics and multiturn charge-exchange injection into the fast cycling synchrotron for the SNS. *IEEE T. Nucl. Sci.* **28**, 3085–3087 (1981). <https://doi.org/10.1109/TNS.1981.4332017>
7. W.P. Chai, J.C. Yang, J.W. Xia et al., Stripping accumulation and optimization of HMM synchrotron. *Nucl. Instrum. Methods A* **763**, 272–277 (2014). <https://doi.org/10.1016/j.nima.2014.05.117>
8. W.P. Chai, J.C. Yang, J.W. Xia et al., Design of a compact structure cancer therapy synchrotron. *Nucl. Instrum. Methods A* **756**, 19–22 (2014). <https://doi.org/10.1016/j.nima.2014.04.050>
9. H.P. Jiang, J.L. Liu, H.F. Hao et al., SESRI 300 MeV proton and heavy ion accelerator. In: *Journal of Physics: Conference Series*, vol. 1350, p. 012081 (2019). <https://doi.org/10.1088/1742-6596/1350/1/012081>
10. S. Ruan, J.C. Yang, J.W. Xia et al., The 300 MeV proton and heavy ion accelerator complex for SESRI project in China. *Nucl. Instrum. Methods A* **1007**, 167916 (2023). <https://doi.org/10.1016/j.nima.2022.167916>
11. D.L. Friesel, S.Y. Lee, Status of the IUCF cooler injector synchrotron. In: *Proceedings of the 1997 Particle Accelerator Conference*, vol. 1, pp. 935–937 (1997). <https://doi.org/10.1109/PAC.1997.749886>
12. Z.M. Wang, W. Chen, M.T. Qiu et al., Construction and beam commissioning of a compact proton synchrotron for space radiation environment simulation. *Nucl. Instrum. Methods A* **1027**, 166283 (2022). <https://doi.org/10.1016/j.nima.2021.166283>
13. Z.M. Wang, Y. Yang, W.L. Liu et al., Commissioning of the 7 MeV H⁻ linac injector for a 200 MeV proton synchrotron. *Nucl. Instrum. Methods A* **1040**, 167244 (2022). <https://doi.org/10.1016/j.nima.2022.167244>
14. W.B. Ye, H.J. Yao, S.X. Zheng et al., Multiple energy extraction experiment at XiPAF synchrotron. *Nucl. Instrum. Methods A* **1058**, 168889 (2024). <https://doi.org/10.1016/j.nima.2023.168889>
15. G.R. Li, S.X. Zheng, H.J. Yao et al., Design of a compact ring for proton radiation applications. *Chin. Phys. C* **41**, 017001 (2019). <https://doi.org/10.1088/1674-1137/41/1/017001>
16. S.X. Zheng, Q.Z. Xing, X.L. Guan et al., Overall design and progress of XiPAF project. In: *Proceedings of the 13th Symposium on Accelerator Physics (SAP'17)*, (2017). <https://doi.org/10.18429/JACoW-SAP2017-WECH2>
17. H.J. Yao, X. Guan, Y. Li et al., Beam commissioning of XiPAF synchrotron. In: *Proceedings of the 12th International Particle Accelerator Conference (IPAC21)*; (2021). <https://doi.org/10.18429/JACoW-IPAC2021-MOPAB189>
18. H.J. Yao, H.B. Chen, C. Cheng et al., Design of the 230 MeV proton accelerator for Xi'an proton application facility. In *Proceedings of the 57th ICFA Advanced Beam Dynamics Workshop on High Intensity, High Brightness, and High Power Hadron Beams (HB2016)*. Malmö, Sweden. (2016). <https://doi.org/10.18429/JACoW-HB2016-MOPR006>
19. H.J. Yao, X.L. Guan, G.R. Li et al., H-charge exchange injection for XiPAF synchrotron. In: *Proceedings of HB2016*. Malmö, Sweden. (2016). <https://doi.org/10.18429/JACoW-HB2016-MOPR004>
20. X.Y. Liu, H.J. Yao, Y. Li et al., Synchrotron injection and acceleration commissioning of Xi'an 200 MeV proton application facility. *Modero Appl. Phys.* **14**, 10405 (2023). <https://doi.org/10.12061/j.issn.2095-6223.2023.010405>. (in Chinese)
21. X.Y. Liu, X. Guan, Y. Li et al., Injection optimization and study of XiPAF synchrotron. In: *Proceedings of IPAC2021*, Campinas, SP, Brazil (2021). <https://doi.org/10.18429/JACoW-IPAC2021-TUPAB326>
22. J.F. Ostiguy and J. Holmes, PyORBIT: a python shell for ORBIT. In: *Proceedings of the 2003 Particle Accelerator Conference*, Portland, OR, USA (2003), pp. 3503–3505. <https://doi.org/10.1109/PAC.2003.1289962>
23. A. Shishlo, S. Cousineau, J. Holmes et al., The particle accelerator simulation code PyORBIT. *Procedia. Comput. Sci.* **51**, 1272–1281 (2015). <https://doi.org/10.1016/j.procs.2015.05.312>
24. F. Ballarini, G. Battistoni, M. Brugger et al., The physics of the FLUKA code: recent developments. *Nucl. Instrum. Methods A* **40**, 1339–1349 (2007). <https://doi.org/10.1016/j.asr.2007.05.031>
25. J.M. Barbosa, A.B. Urtula, R. Hirata et al., Thickness evaluation of articulating papers and foils. *J. Esthet. Restor. Dent.* **30**, 70–72 (2017). <https://doi.org/10.1111/jerd.12343>
26. P. Maier-Komor, G. Dollinger, E. Hammann, Thickness calibration of carbon foils. *Nucl. Instrum. Methods A* **303**, 88–93 (1991). [https://doi.org/10.1016/0168-9002\(91\)90768-L](https://doi.org/10.1016/0168-9002(91)90768-L)
27. R. Wang, D. Liu, Foil thickness determination by CBED in the kinematical approximation. *Phys. Stat. Sol. (A)* **99**, 47–55 (1987). <https://doi.org/10.1002/pssa.2210990106>
28. L.C. Hao, M.V. Nhon, C.V. Tao et al., Methods for thin foil thickness determination by using alpha spectroscopy. *Kerntechnik* **75**, 135–137 (2013). <https://doi.org/10.3139/124.110065>
29. P.K. Saha, M. Yoshimoto, H. Hotchi et al., Measurement of continuous degradation of a stripper foil during the operation with 300 kW beam power in the 3-GeV RCS of J-PARC. *J. Radioanal. Nucl. Ch.* **305**, 851–857 (2015). <https://doi.org/10.1007/s10967-015-4023-7>
30. M. Tanabashi, K. Hagiwara et al., Review of particle physics. *Phys. Rev. D.* **98**, 030001 (2018). <https://doi.org/10.1103/PhysRevD.98.030001>
31. Brian J. McParland et al., Mean excitation energy. In: *Medical Radiation Dosimetry*, pp. 405–419, (2013). https://doi.org/10.1007/978-1-4471-5403-7_11
32. J. Yan, J. Wu, Y. Zhang et al., EPICS based beam energy measurement system for proton LINAC. In: *IEEE 3rd Advanced Information Technology, Electronic and Automation Control Conference (IAEAC) in Chongqing, China* (2018). <https://doi.org/10.1109/IAEAC.2018.8577912>
33. T. Watanabe, M. Fujimaki, N. Fukunishi et al., Beam energy and longitudinal beam profile measurement system at the RIBF. In: *5th International Particle Accelerator Conference (IPAC 2014)*. (2014). <https://doi.org/10.18429/JACoW-IPAC2014-THPME136>
34. S. van der Meer, Diagnostics with Schottky noise. In: *Frontiers of Particle Beams; Observation, Diagnosis and Correction: Proceedings of a Topical Course Held by the Joint US-CERN School on Part. Accel. at Anacapri*. (2005)
35. H. Koziol, Beam diagnostics for accelerators. No. CERN-PS-2001-012-DR. (2001)

Springer Nature or its licensor (e.g. a society or other partner) holds exclusive rights to this article under a publishing agreement with the author(s) or other rightsholder(s); author self-archiving of the accepted manuscript version of this article is solely governed by the terms of such publishing agreement and applicable law.